Parallel pumping fine structure at 9.4 GHz for in-plane magnetized yttrium iron garnet thin films

G. Wiese, L. Buxman, P. Kabos,[a] and C. E. Patton
Department of Physics, Colorado State University, Fort Collins, Colorado 80523

(Received 29 July 1993; accepted for publication 29 September 1993)

A fine structure in the parallel pumping spin wave instability absorption has been observed. The data were obtained at 9.4 GHz on a narrow linewidth in-plane magnetized yttrium iron garnet film with a magnetic layer thickness of 15.9 μm. The standard butterfly curve of the spin wave instability threshold microwave field amplitude h_{crit} versus external static magnetic field H_{ext} was constructed from h_{crit} determinations obtained by sweeping the static field at different microwave power levels and measuring the change in microwave loss. For values of H_{ext} below the minimum, h_{crit} position, the loss versus H_{ext} profiles showed a characteristic fine structure previously observed only in spheres. The fine structure spacing was on the order of 5 Oe and the square of the spacing decreased linearly with increasing static field. These fine structure results are in accord with predictions from theory for critical modes at one-half the pump frequency, with the critical mode wave vectors aligned perpendicular to the film plane, and with the wave numbers for these modes quantized as standing spin wave modes for a thin film. Analysis of the fine structure data gives a spin wave exchange stiffness parameter $D_{fs}=(6.0\pm0.9)\times10^{-9}$ Oe cm^2, which agrees within experimental error with the value $D=(5.4\pm0.2)\times10^{-9}$ Oe cm^{-2} obtained from Brillouin light scattering measurements on YIG spheres. The standing wave critical modes are explained in terms of cooperative volume dipole-dipole and shape demagnetizing induced ellipticity for the modes.

I. INTRODUCTION

The parametric excitation of spin waves in ferrites by the application of a linearly polarized microwave magnetic field parallel to the external static magnetic field was first reported in 1960 by Schlömann *et al.*[1] and Morgenthaler.[2] The excited spin waves are at a frequency ω_k which is at one-half the microwave pump frequency ω_p and the parametric spin wave excitation occurs only if the microwave field amplitude h exceeds a certain spin wave instability threshold amplitude h_{crit}. This instability threshold is measured by monitoring the microwave power absorbed by the ferrite sample as the microwave power applied to the sample is increased at fixed static field[1,3] or as the static field is changed at different fixed microwave power levels.[4] As the microwave field amplitude h exceeds h_{crit}, the relative power absorbed by the sample increases abruptly. In this manner, one obtains so-called "butterfly curves" of h_{crit} versus the static external field H_{ext}.

Typical parallel pumping butterfly curves for narrow linewidth single crystal ferrites have an h_{crit} which decreases with increasing external static field at low field, shows a more or less pronounced cusp at $H_{ext}=H_{min}$, and then increases to a point of divergence at some cutoff static field H_{cut}.[1,5] This characteristic shape reflects the fact that for a given static field, the instability occurs for the spin wave at $\omega_k=\omega_p/2$ with the lowest threshold. For static fields below the cusp, the minimum threshold modes have a wave vector k which is perpendicular to the static field and a corresponding polar spin wave propagation angle θ_k of 90°. In this field range, therefore, the minimum threshold modes follow the upper $\theta_k=90°$ branch of the spin wave band and the wave number k of the minimum threshold modes gradually decreases with increasing field to a nominal value near $k\approx0$ at the cusp point. The cusp point corresponds, therefore, to the value of H_{ext} for which the upper $\theta_k=90°$ branch of the spin wave band at low wave number crosses the $\omega_p/2$ frequency point. For the external static field range from the cusp point to cutoff, the wave number remains at $k\approx0$ and θ_k decreases from 90° to 0°. For static external fields above H_{cut}, there are no available spin wave modes at $\omega_k=\omega_p/2$ and the threshold diverges. The basic parallel pumping process for ferrites is discussed extensively in the literature.[1,6,7]

A new feature of the parallel pumping process in narrow linewidth single crystal yttrium iron garnet (YIG) was observed in 1971 by Andlauer *et al.*[8] and Jantz *et al.*,[9] in the course of careful measurements on highly polished, stress free single crystal YIG submillimeter diameter spheres at 9 GHz. The h_{crit} data were obtained by sweeping the static field at different microwave power levels and measuring the microwave loss versus H_{ext} profiles, following Ref. 4. The loss profiles were obtained on an expanded sweep scale on the order of a few Oe. These workers found, in addition to the gradual decrease in the threshold h_{crit} with increasing H_{ext} for fields below the cusp field, a very regular series of closely spaced narrow peaks in the microwave loss versus H_{ext} profiles and referred to these profiles as "fine structure." This fine structure consisted of a series of extremely narrow peaks with widths down to 0.003 Oe and spacings on the order of 0.01 Oe. The fine structure was explained by assuming that the wave numbers of the excited $\theta_k=90°$ spin waves were quantized in integer multiples of π/d_s, where d_s denotes the diameter of the YIG

[a]On leave from the Slovak Technical University, Bratislava, Slovakia.

 0021-8979/94/75(2)/1041/6/$6.00 © 1994 American Institute of Physics

sphere. A more detailed analysis of this fine structure in terms of the true spherical eigenmodes of the sphere[10] showed that the effective wave numbers of the true spherical modes are quantized in integer multiples of π/d_s and gave additional support to the Jantz model. Fine structure related to the discrete nature of the spin wave spectrum in the decline of the ferromagnetic resonance absorption with increasing power level has been observed and explained much earlier by Schlömann and Green.[11,12]

The availability in recent years of high quality YIG thin films grown on single crystal gadolinium gallium garnet substrates by the liquid phase epitaxy technique[13] and prospects for YIG film microwave devices,[14] has led to a revival of interest in the study of nonlinear microwave processes in such films.[15–23] With the exception of Ref. 16, the analyses of these results, however, were generally based on bulk theory, following Suhl,[24] Schlömann,[25] and Patton.[26–29] However, from the works of Damon and Eshbach,[30] Sparks,[31], Wolfram and DeWames,[32] Vendik *et al.*,[33] Kalinikos,[34] and others, it is well known that the dynamic modes for magnetic thin films can be quite different from the corresponding modes in bulk samples. In particular, the components of the wave vector perpendicular to the plane of the film is quantized in integer multiples of π/d, where d denotes the film thickness. Vendik *et al.*[33] also considered the theoretical problem of parallel pumping in thin films in terms of the quantized spin wave modes for the structure and predicted multiple minimum threshold cusp points corresponding to standing spin wave modes across the film thickness. Based on the formalism of Ref. 10, Wiese[35] has developed a theory for spin wave instability processes in thin films as well. On the basis of the theory in Ref. 35, Wiese *et al.*[36] have measured and successfully explained butterfly curves for subsidiary absorption processes in thin YIG films.

Up to now, there has been no reported study of the fine structure phenomena in YIG thin films. Because of the well defined mode quantization indicated above, thin films represent ideal structures in which to observe such effects. In fact, Kalinikos *et al.*[16] have measured parallel pumping butterfly curves at 9.4 GHz for in-plane magnetized 0.5 μm YIG films. The h_{crit} values were obtained by increasing the microwave power at fixed static field and observing the onset for nonlinear loss. These workers obtained multiple butterfly curves with cusp points on the order of 200 Oe apart. They interpreted these different curves as due to the different quantized thickness modes of the film, essentially the standing spin wave modes at $\omega_k=\omega_p/2$ as predicted in Ref. 33. This result suggests that the Jantz type fine structure could be readily observed for somewhat thicker films by sweeping the static field at constant microwave power, the procedure used in Refs. 8 and 9.

This study presents the results of such parallel pumping measurements on an in-plane magnetized YIG film at 9.4 GHz. The butterfly curve data follow the basic scenario outlined above. The data show the expected characteristic fine structure for the entire range of static fields below the butterfly curve minimum. Analysis of the fine structure spacing δH as a function of static field indicates that the minimum threshold modes are spin waves with $\theta_k=90°$, as expected, wave vectors which are *perpendicular* to the film plane, and wave numbers which are quantized in integer multiples of π/d. Analysis of the variation of the measured δ spacings with H_{ext} gives a spin wave exchange stiffness parameter $D_{fs}=(6.0\pm0.9)\times10^{-9}$ Oe cm^2. This value agrees within experimental error with the value $D=(5.4\pm0.2)\times10^{-9}$ Oe cm^2 obtained from Brillouin light scattering measurements on YIG spheres.[37]

II. FILM PROPERTIES, EXPERIMENT, AND RESULTS

The microwave loss profiles were measured on a (111) plane rectangular shaped 2.5 mm$\times$2.7 mm YIG film at 9.4 GHz and room temperature. The YIG film, provided by the Westinghouse Research and Development Center, Pittsburgh, Pennsylvania, was grown by conventional liquid phase epitaxy techniques on a gadolinium gallium garnet substrate. The nominal film thickness, estimated from the growth rate and time, was 12.8 μm. The film had a narrow ferromagnetic resonance half power linewidth of about 0.5 Oe at 10 GHz. All measurements were made for the external static field H_{ext} in the film plane.

An accurate determination of the YIG film thickness will be important for the analysis and discussion given below. The thickness of the YIG layer was determined by an additional microwave experiment, based on the field spacing of the low power surface magnetostatic mode resonances when a rectangular in-plane magnetized film is excited by a narrow stripline transducer placed on top of the film, and the static magnetic field is parallel to the stripline.[38] With the stripline placed in the center of and parallel to one side of the rectangular film, the excited standing surface modes have in-plane wavenumbers which are quantized according to $k_s=n\pi/L$, where L is the length of the edge perpendicular to the stripline and n is an odd integer. Following this technique, stripline measurements at 3 GHz yielded a magnetic film thickness of 15.9 $\pm$0.8 μm, somewhat larger than the nominal growth estimated thickness of 12.8 μm.

The parallel pumping measurements were made at room temperature with a modified Varian 4500 EPR spectrometer and a TE102 rectangular cavity of moderate quality factor $Q=3100$. The 9.4 GHz cavity was undercoupled and had a reflection coefficient of -9.54 dB at cavity resonance. The thin film sample was placed in the center of the cavity with the microwave field in-plane. The cavity was placed in the gap of the electromagnet so that the linearly polarized microwave magnetic field was parallel to the static field.

The details of the measurement procedure were the same as used by Patton and Jantz.[39] The external magnetic field was swept at constant microwave power incident on the cavity and the field point for the abrupt increase in microwave loss which marks the instability threshold was measured. Such a loss profile, properly calibrated, yields a pair of H_{ext} and h_{crit} values. This procedure was repeated for a large number of power levels and the calibrated data were used to construct the butterfly curve. The calibration to obtain the amplitude of the linearly polarized micro-

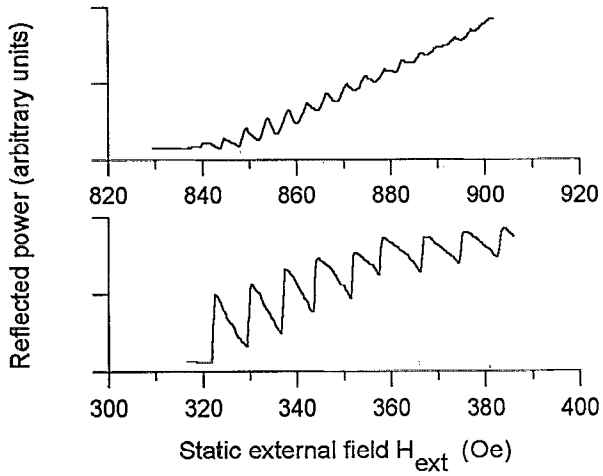

FIG. 1. Profiles of the parallel pumping microwave loss vs in-plane static field H_{ext} for two different incident power levels and static field ranges. The data are for a 15.9-μm-thick yttrium iron garnet (YIG) field and a pump frequency of 9.4 GHz. Profile (a) is for an incident power of 95 mW and a microwave field amplitude of 0.73 Oe. Profile (b) is for a power of 192 mW and a microwave field of 1.04 Oe.

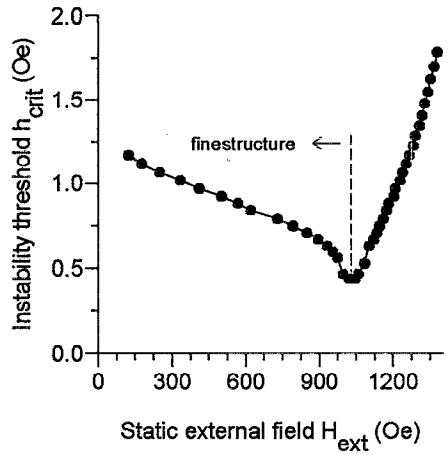

FIG. 2. Parallel pumping butterfly curve of the spin wave instability threshold microwave field amplitude h_{crit} vs static field H_{ext}. The data are for a 15.9-μm-thick yttrium iron garnet (YIG) film and a pump frequency of 9.4 GHz. The static and linearly polarized microwave fields are colinear and in-plane.

wave field as a function of the microwave power was obtained from the usual empty cavity approximation and electromagnetic theory. The cavity calibration constant was 5.625 Oe^2/W.

Typical loss versus static field H_{ext} profiles for two different ranges of the static field are shown in Fig. 1. Profile (a) is for an incident power of 95 mW and profile (b) is for an incident power of 192 mW. These powers correspond to microwave field amplitudes of 0.73 and 1.04 Oe, respectively. The microwave power levels for these two scans were chosen in such a way that the onset of microwave absorption starts at close to the left edge of the scan. This means that the microwave power above the onset of loss is only slightly above threshold. The onset of loss for profile (a) is at a static field of about 841 Oe, corresponding to an (h_{crit}, H_{ext}) point at (0.73 Oe, 841 Oe). For profile (b) the (h_{crit}, H_{ext}) point is at (1.04 Oe, 322 Oe). In addition to the loss onset points which serve to determine h_{crit}, the profiles also show a regular structure for static fields above the loss onset. This regular structure corresponds to the "fine structure" discussed in the introduction. The data in Fig. 1 represent the first observation of such fine structure in thin magnetic films. The spacing of the fine structure for profile (a) is about 4 Oe. For profile (b), the spacing is about 8 Oe. It is significant to note that this spacing decreases with increasing field.

Figure 2 shows the resulting parallel pumping butterfly curve constructed from loss profiles similar to the profiles shown in Fig. 1. The butterfly curve shows the basic features outlined in the introduction, with values of h_{crit} which decrease, with increasing H_{ext} at low field, a cusp point, and an h_{crit} which increases for static fields above the cusp point. The available microwave power was too low to reach the butterfly curve cutoff at $H_{crit}=1600$ Oe. The value of h_{crit} at the cusp point is about 0.5 Oe, corresponding to a spin wave linewidth parameter ΔH_k of 0.26 Oe. An intrinsic linewidth of 0.5 Oe at 4.9 GHz, one-half the pump frequency, is quite reasonable for high quality single crystal YIG films.

Turn now to the fine structure spacing results. As already indicated, the fine structure shown for the profiles in Fig. 1 was obtained only for ranges of the static field below the cusp point in Fig. 2. Over this low field range, the fine structure spacing was found to decrease with increasing static field. Guided by theoretical considerations to be discussed below, it was found that the *square* of fine structure spacing δH is a decreasing linear function of H_{ext}. This experimental result is shown in Fig. 3, where the square of the measured spacing $(\delta H)^2$, is plotted versus the static external field, H_{ext}. Fine structure spacings below about 3 Oe or so were too small to be resolved. While some scatter is evident from the plot, the linear dependence is quite

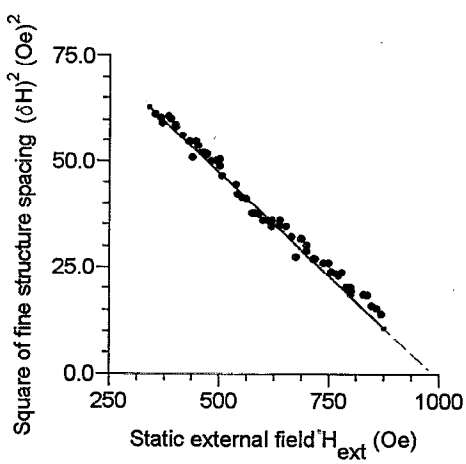

FIG. 3. Square of the fine structure field spacing δH as a function of the static external field H_{ext}. The spacings were measured from the fine structure in the microwave loss vs H_{ext} profiles similar to those shown in Fig. 1 for a 15.9-μm-thick yttrium iron garnet (YIG) film and a pump frequency of 9.4 GHz. The filled circles represent the measurements. The solid line represents a straight line best fit to the data.

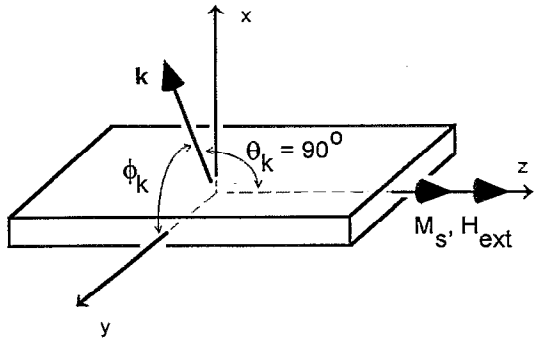

FIG. 4. Schematic diagram of the thin film geometry. The film is in the y-z plane, the external static field $\mathbf{H}_{ext}$ and the static magnetization $\mathbf{M}_s$ are in the z direction, the critical mode spin wave wave vector $\mathbf{k}$ is at a polar angle $\theta_k=90°$ relative to $\mathbf{H}_{ext}$ and a general azimuthal angle ϕ_k with respect to the in-plane y axis.

clear. The straight line in Fig. 3 represents a straight line best fit to the data. This fit extrapolates to $(\delta H)^2=0$ at $H_{ext}\approx 1000$ Oe, a field close to the butterfly curve minimum. It is significant that no fine structure was found for H_{ext} values above the butterfly curve minimum.

III. ANALYSIS AND DISCUSSION

The butterfly curve data in Fig. 2 can be modeled according to the theory for isotropic spheres in the usual way, by assuming some operational form for the wave number k and polar angle θ_k dependence of the spin wave linewidth. Such modeling yields basically the same results obtained for YIG spheres.[27,29,30] One obtains a k-dependent spin wave linewidth function of the form

$$\Delta H_k = A + B\sin^2(2\theta_k) + Ck\,, \tag{1}$$

and minimum threshold modes which follow the scenario described in the introduction. The basic critical mode properties are: (1) $\theta_k=90°$ and k decreasing with increasing static field for fields below the minimum h_{crit} cusp point. (2) k nominally equal to zero and a θ_k which decreased smoothly from 90° to zero as the field moves from the cusp position to the high h_{crit} cutoff.

For sphere samples due to spherical symmetry, one would have *no* dependence of the threshold on the azimuthal spin wave angle ϕ_k. One question pertinent to the present thin film case, however, is the *relative* orientation of the critical mode wave vector $\mathbf{k}$ relative to the film plane. The wave vector-thin film geometry is shown schematically in Fig. 4. The film is in the y-z plane and the external static field $\mathbf{H}_{ext}$ and static magnetization vector $\mathbf{M}_s$ are aligned along the z direction. The critical mode wave vector $\mathbf{k}$ is shown at $\theta_k=90°$ and at a general angle ϕ_k relative to the in-plane $\phi_k=0°$ direction. It is clear from the diagram in Fig. 4(a) that one can have $\theta_k=90°$ with $\mathbf{k}$ in-plane, $\mathbf{k}$ perpendicular to the film plane, or $\mathbf{k}$ in any direction in between. For the convention in Fig. 4, the perpendicular-to-plane propagation direction corresponds to $\phi_k=90°$. The present data show clear fine structure for *all* static fields *below* the cusp point, corresponding to $\theta_k=90°$. If this fine structure is associated with standing modes across the film thickness, this implies that the critical mode wave vector $\mathbf{k}$ is perpendicular to the film plane and with $\phi_k=90°$.

Based on the above conditions for the critical modes below the cusp point, namely, $\omega_k=\omega_p/2$, $\theta_k=90°$, and $\phi_k=90°$, and assuming that the critical mode wave number k is quantized according to $k=n\pi/d$, where n is an integer, one can calculate explicitly the field spacing δH for the critical modes. One starts with the usual infinite medium spin wave dispersion relation,

$$\omega_k^2=\gamma^2(H_i+Dk^2)(H_i+Dk^2+4\pi M_s\sin^2\theta_k)\,, \tag{2}$$

where γ is the gyromagnetic ratio, H_i is the static internal field, D is the spin-wave exchange stiffness constant, and $4\pi M_s$ denotes the saturation induction for the material. For the present thin film case, the internal static field H_i and the external static field H_{ext} are equal. Under the additional assumption that $n\gg 1$ is valid, the separation between adjacent modes is obtained as

$$\delta H=\sqrt{C_\delta - D\left(\frac{2\pi}{d}\right)^2}\,H_{ext}\,, \tag{3}$$

where C_δ is a constant. Equation (3) is the basis for the display format in Fig. 3, $(\delta H)^2$ vs H_{ext}.

From Eq. (3), the slope of the straight line best fit to the data in Fig. 3 should be negative and equal to $-D(2\pi/d)^2$. This means that if the film thickness d is known, the measured slope can be used to determine the spin wave exchange stiffness parameter D. Comparison of the D value obtained from the above determination with known D values from other methods provides a measure of the validity of the perpendicular-to-film $\mathbf{k}$ vector/standing mode model. The slope of the straight line best fit in Fig. 3 is -0.094 ± 0.005 Oe. Based on the magnetic film thickness determination $d=15.9\pm0.8$ μm, Eq. (3) yields a spin wave stiffness constant $D_{fs}=(6.0\pm0.9)\times10^{-9}$ Oe cm^2. The generally accepted value of D from Brillouin light scattering measurements of the spin wave dispersion on YIG spheres,[37] is $D=(5.4\pm0.2)\times10^{-9}$ Oe cm^2. The D_{fit} value is in agreement with the accepted D value within experimental error. This confirms the underlying assumption for the analysis that the critical mode wave vectors are perpendicular to the film plane. Note that the value obtained for D_{fs} is extremely sensitive to the film thickness d. If the d value estimated from the growth process, 12.8 μm, is used, one obtains an unacceptably low D_{fs} value of 3.9×10^{-9} Oe cm^2.

The condition $n\gg1$ can also be checked. From Eq. (2), with $\omega_k=\omega_p/2$ and $\theta_k=90°$, one obtains critical mode k values at $H_{ext}=350$ Oe and 850 Oe, the two limits for the data in Fig. 3, as 4.1×10^5 cm^{-1} and 1.8×10^5 cm^{-1}, respectively. These wave numbers correspond, to $n=210$ and $n=90$, respectively. The $n\gg1$ condition is well satisfied for the range of fields examined.

It is to be emphasized that, so far, the conclusion of $\theta_k=90°$ critical modes which have wave vectors perpendicular to the film plane and $\phi_k=90°$ is purely empirical. The physical basis for this $\phi_k=90°$ preference must be contained in consideration of the spin wave ellipticity. In par-

allel pumping, it is the time dependent longitudinal m_z component of the magnetization at a frequency $2\omega_k$ which couples to the parallel pump microwave field at ω_p. It is this coupling that gives rise to the critical spin wave mode frequency selectivity condition, $\omega_k=\omega_p/2$. The relative size of m_z, moreover, depends on the ellipticity of the precession cones for the spin waves, when viewed classically. When these precession cones are circular, as for parallel spin wave propagation at $\theta_k=0°$, the ellipticity is zero, m_z is zero, and the parallel pump threshold diverges. This is the cause of the diverging threshold at cutoff discussed in the introduction. For spin waves in large, isotropic samples, the ellipticity is maximum for perpendicular propagation, at $\theta_k=90°$. For a general propagation direction in such materials, this ellipticity scales with $\sin^2\theta_k$ and is connected with the nonzero volume dipole-dipole energy density for spin waves with $\theta_k\neq 0°$. The major axis of the precession cone ellipse is parallel to the direction defined by the vector product $\mathbf{M}_s\times\mathbf{k}$.

The critical mode preference for out-of-plane propagation for in-plane magnetized thin films is due to the additional effect of the thin film geometry on the spin wave ellipticity. It is well known that the precession cones for the long wavelength normal modes in thin films are elliptical, due mainly to the effect of the large perpendicular direction demagnetizing factor in keeping the precessing magnetization vector in-plane. The thin film geometry has a similar effect on the spin wave modes, albeit less pronounced. As the spin wave k value increases and the spin wave wavelength becomes very much smaller than the film thickness, the effect of shape on the spin wave ellipticity becomes vanishingly small.

The $\phi_k=90°$ critical mode preference, which is the basis of the observed fine structure, derives from the interplay between the volume dipole-dipole effect and the thin film shape effect. The volume dipole-dipole effect promotes an elliptical precession cone with a major axis which is parallel to the vector product $\mathbf{M}_s\times\mathbf{k}$. The thin film shape effect promotes an elliptical precession cone with a major axis which is in-plane. These effects match up for $\phi_k=90°$, but are in opposition for $\phi_k=0°$. The situation is shown schematically in Fig. 5. A thin film is shown in cross section with the external static field $\mathbf{H}_{ext}$ and static magnetization $\mathbf{M}_s$ out of the page. The elliptical precession cone orientations promoted by the volume dipole-dipole interaction for in-plane propagation at $\phi_k=0°$ and for perpendicular propagation at $\phi_k=90°$ are shown by the vertically and horizontally aligned ellipses, respectively. As shown by these diagrams, the ellipse major axes are in-plane for $\phi_k=90°$ and perpendicular to the film plane for $\phi_k=0°$. For $\phi_k=90°$, the thin film shape effect and the volume dipole-dipole effect work together to promote the maximum ellipticity, and hence, the lowest instability threshold.

The above considerations are made quantitative in the somewhat formal theory of Vendik *et al.*[33] and in the analysis of thin YIG film parallel pumping butterfly curve data based on that theory by Kalinikos *et al.*[16] These workers showed that for thin films, the spin waves propagating perpendicular to the film plane become quasi-surface spin

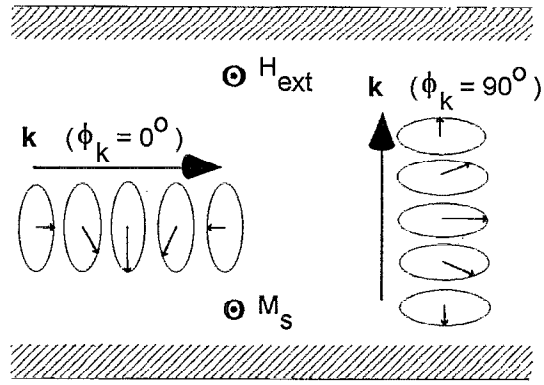

FIG. 5. Schematic diagram of the thin film in cross section. The external static field $\mathbf{H}_{ext}$ and the static magnetization $\mathbf{M}_s$ are directed out of the plane of the page. The two series of ellipses indicate the two different volume dipole-dipole related spin wave elliptical precession cone orientations for two different critical mode propagation directions. In both cases, the wave vector $\mathbf{k}$ is perpendicular to $\mathbf{H}_{ext}$, corresponding to $\theta_k=90°$. Case (a) $\mathbf{k}$ is in-plane, corresponding to $\phi_k=0°$, and the precession cones have major axes which are perpendicular to the film plane. Case (b): $\mathbf{k}$ is perpendicular to the film plane, corresponding to $\phi_k=90°$, and the precession cones have major axes which are parallel to the film plane.

waves which have a larger ellipticity and therefore a stronger parallel pumping coupling coefficient than do the corresponding $\phi_k=90°$ spin-waves propagating in the film plane. For the relatively thin 0.5 μm films used in Ref. 16, there would be relatively few standing mode half wavelengths across the film cross section for the range of k values applicable to the low field part of the butterfly curve in Fig. 1 the thin film related ellipticity effect would be fairly large. The critical mode quantized standing wave k values would be spaced apart by about 200 Oe and would show a pronounced change in threshold with field. These effects lead to the very pronounced series of butterfly curve minima shown in Ref. 16. For thicker films and higher order standing modes, the bulk ellipticity effect would be reduced and the butterfly curve minima would be closer and less pronounced. In the course of measurements made by sweeping the static field at constant microwave power, the standing modes would lead to the type of fine structure shown in Fig. 1.

This discussion would not be complete without comment on possible anisotropy effects. The effect of magnetocrystalline anisotropy on the parallel pump threshold has been examined by Patton.[27–29] Reference 28 evaluated the effect of cubic magnetocrystalline anisotropy on the coupling coefficient for an arbitrary pumping configuration in a ferrite ellipsoid saturated along one principal axis. References 27 and 29 explicitly consider parallel pumping in a [110] direction for an in-plane magnetized (110) slab and shows that the effect of anisotropy promotes a critical mode preference for different values of ϕ_k, depending on the size of the cubic anisotropy, sample shape, external magnetic field, spin wave linewidth k dependence, and orientation. While the theory predicts, under certain circumstances, a continuous shift in the critical mode ϕ_k value

with field, the data showed a bistable effect with the critical modes only at either $\phi_k=0°$ or $\phi_k=90°$.

While a detailed discussion of anisotropy effects is beyond the scope of this article, Patton's theory applied to (111) films yields the following: A (111) plane YIG film has six [110] directions in the film plane at angles of 60° to each other. The parallel pump coupling does depend on ϕ_k and the value of ϕ_k for the critical minimum threshold modes also changes with field direction. Specifically, anisotropy promotes critical spin waves at $\phi_k=0°$ when the in-plane static field is between two [110] directions and at $\phi_k=35.26°$ when the field is along a [110] direction. As in the considerations given above, the anisotropy dependences are also due to ellipticity. The change in coupling between these two cases, however, is only 1% or so. In the experiment, one observes *no change* in the fine structure for different in-plane field directions and no change in the slope of the $(\delta H)^2$ vs H_{ext} data. Given this lack of anisotropy in the observed fine structure and the self consistency between the fine structure spacings and the $\phi_k=90°$ assumption, it appears that anisotropy effects cannot explain the experimental results.

ACKNOWLEDGMENTS

Dr. G. Wiese was supported in part on a postdoctoral fellowship from the Deutsche Forschungsgemeinschaft, Bonn, Germany. The YIG films were kindly provided by Dr. J. D. Adam, Westinghouse Research Laboratories, Pittsburgh, Pennsylvania. The research was supported in part by the United States Office of Naval Research, Grant N00014-90-J-4078, the National Science Foundation, Grant DMR-89211761, and the United States Army Research Office, Grant DAAL03-91-G-0327.

[1] E. Schlömann, J. J. Green, and U. Milano, J. Appl. Phys. 31, 386S (1960).
[2] F. R. Morgenthaler, J. Appl. Phys. **31**, 95S (1960).
[3] J. J. Green and T. Kohane, SCP Solid State Technol. August, p. 46 (1964).
[4] W. E. Courtney and J. B. Clarricoats, J. Appl. Phys. **34**, 1279 (1963).
[5] E. Schlömann, J. Phys. Soc. Jpn. **17**, Suppl B-I, 406 (1962).
[6] R. W. Damon, "Ferromagnetic Resonance at High Power," in *Magnetism*, Volume I, edited by G. T. Rado and H. Suhl (Academic, New York, 1963), p. 595.
[7] M. Chen and C. E. Patton, "Spin Wave Instability Processes in Ferrites," in *Nonlinear Phenomena and Chaos in Magnetic Materials*, edited by P. E. Wigen (World Scientific, Singapore, 1993).
[8] B. Andlauer, W. Jantz, and J. Schneider, AIP Conference Proceedings No. 5, *Magnetism and Magnetic Materials-1971* 17th Annual Conference, Chicago, edited by C. D. Graham and J. J. Rhyne (American Institute of Physics, New York, 1972), p. 1209.
[9] W. Jantz, J. Schneider, and B. Andlauer, Solid State Commun. **10**, 937 (1972).
[10] G. Wiese, Z. Phys. B **82**, 453 (1991).
[11] E. Schlömann and J. J. Green, Phys. Rev. Lett. **3**, 129 (1959).
[12] E. Schlömann, Phys. Rev. **116**, 828 (1959).
[13] M. Shone, Circuits, Systems, and Signal Processing **4**, 89 (1985).
[14] Circuits, Systems, and Signal Processing **4**, 1-2 (1985). (Special issue, "Magnetostatic Waves and Applications to Signal Processing").
[15] W. Wettling, W. D. Wilber, P. Kabos, and C. E. Patton, Phys. Rev. Lett. **51**, 1680 (1983).
[16] B. A. Kalinikos, N. G. Kovshikov, and N. V. Kozhus, Sov. Phys. Solid State **27**, 1681 (1986). [Fiz. Tverd. Tela (Leningrad) **27**, 2794 (1985)].
[17] Y. T. Zhang, C. E. Patton, and M. V. Kogekar, IEEE Trans. Magn. **22**, 993 (1986).
[18] G. Srinivasan and C. E. Patton, J. Appl. Phys. **61**, 2318 (1987).
[19] Y. T. Zhang, C. E. Patton, and G. Srinivasan, J. Appl. Phys. **63**, 5433 (1988).
[20] W. D. Wilber, J. G. Booth, C. E. Patton, G. Srinivasan, and R. W. Cross. J. Appl. Phys. **64**, 5477 (1988).
[21] M. Chen, C. E. Patton, G. Srinivasan, and Y. T. Zhang, IEEE Trans. Magn. **25**, 3485 (1989).
[22] G. Srinivasan, M. Chen, and C. E. Patton, J. Appl. Phys. **64**, 5480 (1989).
[23] R. W. Cross, C. E. Patton, G. Srinivasan, J. G. Booth, and M. Chen, J. Appl. Phys. **69**, 1569 (1991).
[24] H. Suhl, J. Phys. Chem. Solids **1**, 209 (1957).
[25] E. Schlömann, Technical Report **R-48**, Research Division, Raytheon Company, Waltham, Massachusetts, 1959 (unpublished).
[26] C. E. Patton, J. Appl. Phys. **40**, 2837 (1969).
[27] C. E. Patton and W. Jantz, IEEE Trans. Magn. **14**, 698 (1978).
[28] C. E. Patton, Phys. Status Solidi B **92**, 211 (1979).
[29] C. E. Patton, Phys. Status Solidi B **93**, 63 (1979).
[30] R. W. Damon and J. R. Eshbach, J. Phys. Chem. Solids **19**, 308 (1961).
[31] M. Sparks, Phys. Rev. B **1**, 3831 (1970).
[32] T. Wolfram and R. E. DeWames, Prog. Surf. Sci. **2**, 233 (1972).
[33] O. G. Vendik, B. A. Kalinikos, and D. N. Chartorizhskii, Sov. Phys. Solid State **19**, 222 (1977). [Fiz. Tverd. Tela (Leningrad) **19**, 387 (1977)].
[34] B. A. Kalinikos, IEE Proc. **127**, (Pt. H, No. 1) 4 (1980).
[35] G. Wiese, Z. Phys. B **91**, 57 (1993).
[36] G. Wiese, P. Kabos, and C. E. Patton, J. Appl. Phys. **74**, 1218 (1993).
[37] J. R. Sandercock and W. Wettling, Solid State Commun. **13**, 1729 (1973).
[38] J. Barak and U. Lachish, J. Appl. Phys. **65**, 1652 (1989).
[39] C. E. Patton and W. Jantz, J. Appl. Phys. **50**, 7082 (1979).
[40] Y. H. Liu and C. E. Patton, J. Appl. Phys. **53**, 5116 (1982).